The Astrophysical Journal, 681:680–692, 2008 July 1

SOLAR ROTATION RATE AND ITS GRADIENTS DURING CYCLE 23

H. M. Antia
Tata Institute of Fundamental Research, Homi Bhabha Road, Mumbai 400005, India; antia@tifr.res.in

Sarbani Basu
Astronomy Department, Yale University, P. O. Box 208101, New Haven, CT 06520-8101; basu@astro.yale.edu

and

S. M. Chitre
Centre for Basic Sciences, University of Mumbai, Mumbai 400098, India; kumarchitre@gmail.com
Received 2008 January 29; accepted 2008 March 21

ABSTRACT

Available helioseismic data now span almost the entire solar activity cycle 23, making it possible to study solar-cycle-related changes of the solar rotation rate in detail. In this paper we study how the solar rotation rate, in particular, the zonal flows, change with time. In addition to the zonal flows that show a well-known pattern in the solar convection zone, we also study changes in the radial and latitudinal gradients of the rotation rate, particularly in the shear layer that is present in the immediate subsurface layers of the Sun. In the case of the zonal flow pattern, we find that the band indicating fast rotating region close to the equator seems to have bifurcated around 2005. Our investigation of the rotation rate gradients shows that the relative variation in the rotation rate gradients is about 20% or more of their average values, which is much larger than the relative variation in the rotation rate itself. These results can be used to test predictions of various solar dynamo models.

Subject headings: Sun: interior — Sun: oscillations — Sun: rotation

1. INTRODUCTION

Helioseismology enables us to study dynamics of the solar interior (e.g., Thompson et al. 1996; Schou et al. 1998). Early results have shown that the differential rotation seen at the solar surface persists until the base of the convection zone and becomes nearly uniform in the radiative interior. Also seen were two shear layers, one near the surface and the other near the base of the convection zone. The latter, which is referred to as the tachocline (Spiegel & Zahn 1992), is generally believed to be the seat of the solar dynamo. Superposed on the relatively smooth latitudinal variation are alternating bands of slightly faster and slower rotation (Kosovichev & Schou 1997).

Data for the last 12 years, covering most of the solar cycle 23, are now available from the Global Oscillation Network Group (GONG) project and the Michelson Doppler Imager (MDI) instrument on board *SOHO*. As a result, it is now possible to study temporal variations of solar dynamics in detail. Early works that used subsets of the data (e.g., Kosovichev & Schou 1997; Schou 1999; Howe et al. 2000a; Antia & Basu 2000) had already established that there is significant variation in the rotation rate of the solar interior. The temporal variation manifests as a system of bands with faster or slower than average rotation rate at fixed depths in the upper layers of the convection zone. And particularly at low latitudes, the zonal flow bands appear to migrate toward the equator with time and appear to be similar in character to the torsional oscillations discovered in the solar surface rotation rate (Howard & LaBonte 1980; Ulrich et al. 1988; Snodgrass 1992). A subsequent work (Antia & Basu 2001) found that in addition to this pattern at low latitudes, there is another system of zonal flow bands at high latitudes (>45°) that migrate toward the poles as the solar cycle progresses. With accumulation of more seismic data it has now become clear that these zonal flows penetrate through most of the convection zone (Vorontsov et al. 2002; Basu & Antia 2003, 2006; Howe et al. 2006b). Since the errors in the results obtained by inversions increase with depth, it is not yet clear whether there is any significant temporal variation in the tachocline region near the base of the convection zone—a region in which the solar dynamo is believed to be operating. Howe et al. (2000b, 2007) reported a 1.3 yr oscillation in the equatorial region around $r = 0.72\,R_\odot$ during the rising phase of the solar cycle, but that has not been confirmed by other studies (e.g., Antia & Basu 2001; Basu & Antia 2003).

The origin of torsional oscillations or zonal flows is not fully understood, but since the zonal flow banded structure and the magnetic activity pattern seem to be closely related, it is generally believed that zonal flows arise from a nonlinear interaction between magnetic fields and differential rotation. Thus, the properties of solar zonal flows should provide a constraint on theories of the solar dynamo. Most dynamo models are kinematic, where the velocity field is specified; such models do not yield any information about temporal variations in the velocity field. However, there are some nonkinematic dynamo models that include the Lorentz force feedback on differential rotation, and these have been used to explain the zonal flow patterns. Covas et al. (2000, 2004), for example, considered an axisymmetric mean-field dynamo model to study temporal variations of the rotation rate and of magnetic fields in the solar interior. They found temporal variations in the rotation rate that are qualitatively similar to the zonal flow pattern inferred from the seismic data. Spruit (2003) suggested that thermal fluctuations due to enhanced emission of radiation by small-scale magnetic fields can drive the zonal flow pattern. His model produces zonal flows with amplitudes that decrease with increasing depth. Lanza (2007) attempted to find the source of the zonal flow pattern by using a model for angular momentum transport in the convection zone and by comparing the results with observed patterns. His preliminary results led to constraints on the amplitude, phase, and location of the perturbations responsible for the observed torsional oscillations. Rempel (2007) found that the poleward moving branch of zonal flows at

high latitude may be explained as a response of the coupled differential rotation/meridional flow system to periodic forcing in midlatitudes by either Lorentz force or thermal perturbations, with thermal fluctuations very likely playing a role in the low-latitude equatorward moving branch of the zonal flow.

Most seismic studies hitherto have investigated temporal variations in the rotation rate itself. For the solar dynamo models, however, spatial gradients of this angular velocity are more important. Although the radial gradient of the rotation rate in the outer shear layer has been studied by Schou et al. (1998), Basu & Antia (2001), and Corbard & Thompson (2002), etc., a detailed study of the temporal variations of both the radial and latitudinal gradients has not been undertaken so far. This motivated us to further investigate changes in both the radial and the latitudinal gradients of the solar rotation rate with a view to studying temporal variations of the shear pattern. We also study the time derivative of the rotation velocity, which should relate to the driving forces that are possibly responsible for the zonal flow pattern. The rest of this paper is organized as follows: we summarize the data and the analysis technique in § 2; our results are described in § 3, and the discussion of our results, along with conclusions, is given in § 4.

2. DATA AND TECHNIQUE

We use data obtained by the GONG (Hill et al. 1996) and MDI (Schou 1999) projects in the present work. These data sets consist of the mean frequency and the splitting coefficients for different (n, ℓ) multiplets. Only the odd-order splitting coefficients are required for determining the rotation rate in the solar interior (e.g., Ritzwoller & Lavely 1991). These splitting coefficients are sensitive only to the north-south symmetric component of the rotation rate, and hence, that is the only component that can be determined with these data. Consequently, all results shown in this work are symmetric about the equator. There could be an antisymmetric component of rotation present in the Sun, but that cannot be analyzed using the global-mode data used in this work. We use 120 data sets from GONG, each set covering a period of 108 days. The first set starts on 1995 May 7, and the last set ends on 2007 May 15, with a spacing of 36 days between consecutive data sets. Thus, there is a considerable overlap between neighboring data sets. The GONG data sets include only *p*-modes up to $\ell = 150$, and we use all modes with frequencies between 1 and 3.5 mHz. The MDI data sets consist of 56 nonoverlapping sets each obtained from observations taken over a period of 72 days. The first set begins on 1996 May 1, and the last set ends on 2007 October 6. Contact with the *SOHO* satellite was lost during 1998 June, and the satellite was finally recovered during 1999 February. During this period there is only one data set, and that covered a period of 60 days. The MDI data sets include *f*-modes up to $\ell = 300$ and *p*-modes up to $\ell \approx 200$. We use all modes with frequencies between 1 and 3 mHz. Since the higher frequency modes often cause problems, they have not been included in the analysis. The higher degree modes from MDI are also known to give misleading temporal variations in some cases (e.g., Antia et al. 2003). This is indeed found to be the case for the radial gradient of the rotation rate and is discussed later.

We use a two-dimensional regularized least-squares (2D RLS) inversion technique, as described by Antia et al. (1998), to infer the rotation rate in the solar interior from each of the available data sets. The first eight odd-order splitting coefficients, $a_1, a_3, \ldots, a_{15}$, were used in the inversions. In order to study the time variation of the rotation rate we first determine the Sun's internal rotation rate using each data set, and then take the time average of the results obtained using all data sets at each latitude and depth. Since we treat the GONG and MDI sets separately, we obtain one average result using GONG sets and another using MDI sets. To obtain the time-varying component of rotation, we subtract the mean from the rotation rate at any given epoch. Thus,

$$\delta\Omega(r, \theta, t) = \Omega(r, \theta, t) - \langle \Omega(r, \theta, t) \rangle, \tag{1}$$

where $\Omega(r, \theta, t)$ is the rotation rate as a function of radial distance r, latitude θ, and time t. Here the angle brackets denote the average over the time duration for which data are available. As is the case for the time-averaged rotation, the residual rotation rate is calculated separately for GONG and MDI data sets.

For most parts of this investigation we use the residual rotation velocity, $\delta v_\phi = \delta\Omega r \cos\theta$, rather than the rotation rate $\delta\Omega$. This time-varying component, δv_ϕ, is generally called the zonal flow. The definition of zonal flows is somewhat ambiguous: some authors (e.g., Howard & LaBonte 1980) have defined the zonal flows by subtracting the temporal average of a smooth component of the rotation rate. The smooth component is generally defined using three terms (constant, $\sin^2\theta$, and $\sin^4\theta$) to calculate the latitudinal variation of rotation rate. There is some difference in the resulting pattern in the two cases, as has been described by Antia & Basu (2000). In this work we adopt the definition given by equation (1), where the temporal mean of the full rotation rate is subtracted to obtain the residuals. This definition has been used previously by other investigators too (e.g., Howe et al. 2000a, 2005, 2006b; Antia & Basu 2001; Basu & Antia 2003, 2006).

For the purpose of investigating the spatial gradients of the rotation rate we use Ω rather than v_ϕ and calculate the radial gradient, $\Omega_r \equiv \partial\Omega/\partial r$, as well as the latitudinal gradient, $\Omega_\theta \equiv (1/r)\,\partial\Omega/\partial|\theta|$. These derivatives are computed numerically. Since the inferred zonal flow pattern is symmetric about the equator, the radial gradient is also symmetric. The latitudinal gradient on the other hand is antisymmetric about the equator, and hence it is 0 at the equator. To restore the symmetry of the latitudinal gradient we have defined the gradient with respect to the absolute value of the latitude. With this definition, both Ω_r and Ω_θ are symmetric about the equator. Since the 2D RLS technique used for inversion gives results that are smooth in (r, θ), there is no difficulty in computing these derivatives numerically. The errors in these derivatives are, of course, larger than those in Ω itself. The time-varying component of these derivatives is calculated by differentiating the residual in rotation rate defined by equation (1), i.e., $\delta\Omega_r \equiv \partial\delta\Omega/\partial r$ and $\delta\Omega_\theta \equiv (1/r)\,\partial\delta\Omega/\partial|\theta|$.

We also calculate the derivative of the rotation velocity v_ϕ with respect to time (note that $\partial v_\phi/\partial t = \partial\delta v_\phi/\partial t$), since it is likely to give an indication of the forcing term that drives the zonal flow pattern. For calculating time derivatives numerically we need v_ϕ at different times, which we obtain from independent data sets. It should be noted that since the magnitude of the zonal flow velocity is small, the temporal derivative has significant errors. To get more reliable estimates we smooth δv_ϕ at each latitude and radius by assuming that the temporal variation is periodic with a period of 11 yr. Since the variation is not strictly sinusoidal, we also include a few higher harmonics and fit the following functional form to δv_ϕ:

$$\begin{aligned}\delta v_\phi(r, \theta, t) &= \sum_{k=1}^{k_{\max}} a_k(r, \theta)\sin(k\omega_0 t) + b_k(r, \theta)\cos(k\omega_0 t) \\ &= \sum_{k=1}^{k_{\max}} A_k \sin(k\omega_0 t + \phi_k).\end{aligned} \tag{2}$$

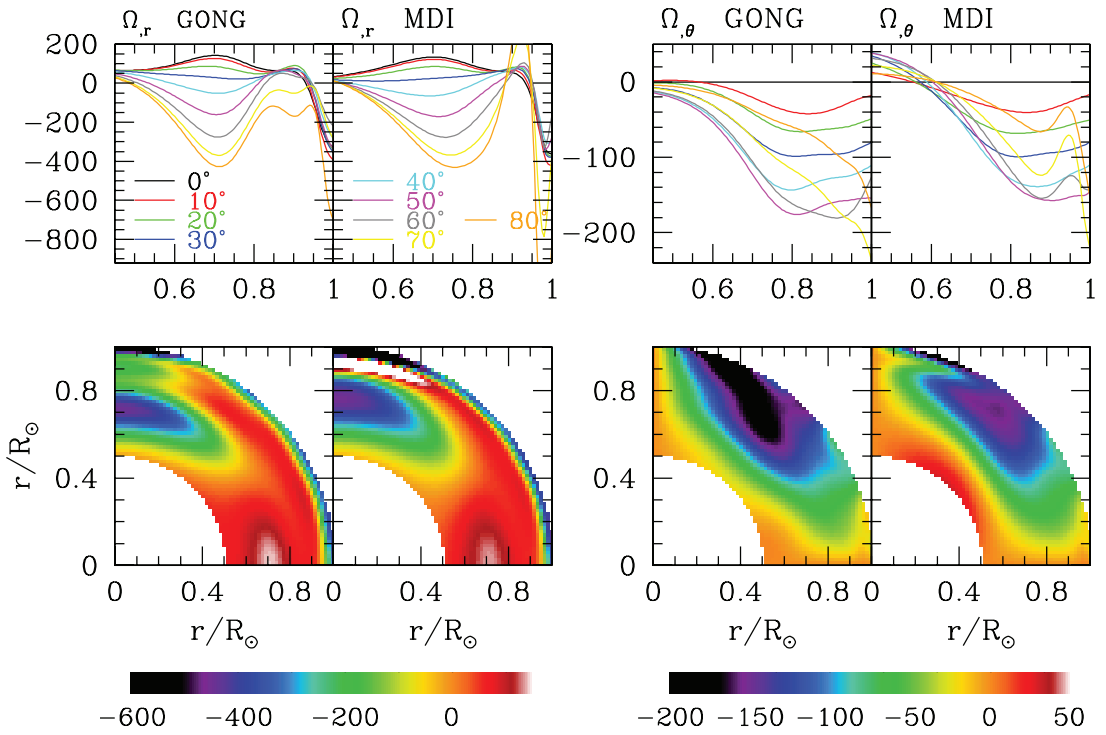

FIG. 1.—Mean radial gradient, Ω_r, and latitudinal gradient, Ω_θ, of the solar rotation rate obtained using GONG and MDI data. Panels in the upper row show the cuts at fixed latitude as a function of radius, while those in the lower row show the same results as color-coded diagrams. All values are in units of nHz $R_\odot^{-1}$.

In the above equation, ω_0 is the basic frequency for the fundamental component, which is assumed to have a period of 11 yr. The coefficients a_k and b_k are determined by a least-squares fit at fixed values of (r, θ). These coefficients determine the amplitude, A_k, and phase, ϕ_k, of the variation at any point defined by the values of (r, θ) for each harmonic of the 11 yr period. We choose time $t = 0$ to be the beginning of GONG data sets, and the phase is measured with respect to that epoch. This zero point is about 1 yr before the minimum phase of solar activity. Three terms are found to be sufficient to fit the data. Similar fits were also used by Vorontsov et al. (2002), Basu & Antia (2003, 2006), and Howe et al. (2005, 2006b). These fits are then used to calculate the time derivative. These fits also enable us to extend the pattern beyond the epochs for which observations exist. These extended patterns are often useful in comparing the observed pattern with those obtained on the basis of dynamo models, since dynamo-model predictions are traditionally shown over a period of 22 yr.

3. RESULTS

The rotation rate in the solar convection zone exhibits temporal variations. Near the solar surface the pattern is observed to be similar to the well-known torsional oscillations detected at the surface. In what follows we describe our results in detail. We include results on the temporal variation, as well as results on the radial, latitudinal, and time derivatives of the rotation rate.

Before discussing temporal variations we examine the time-averaged quantities. Since the mean rotation rate inferred by the inversion of seismic data is well known (e.g., Thompson et al. 1996; Schou et al. 1998), we do not show the results here, but instead we only show the results for the gradients, Ω_r and Ω_θ. The upper panels of Figure 1 show the cuts at fixed latitude, while the lower panels show the color-coded results as a function of both r and θ.

The radial gradient of the solar rotation rate is large in the outer shear layer, as well as in the tachocline, and is small in other regions. Below the outer shear layer, the radial gradient is positive in the low-latitude regions and is negative in all other regions wherever it can be determined reliably. In the outer shear layer we find an average negative gradient of the order of a few hundred nHz $R_\odot^{-1}$, i.e., 10^{-15} m^{-1} s^{-1}. The value of Ω_r is largely independent of latitude in the outer shear layer, except perhaps at very high latitudes. It should be noted that the regularization used in carrying out the inversions smooths out the radial variations near the tachocline region and hence the actual radial gradient in the tachocline region is expected to be much larger. If the tachocline model obtained by Antia et al. (1998) is used to define the rotation rate in the tachocline region, the gradient can be calculated more precisely, and the results obtained using MDI data are shown in Figure 2. It is clear that the gradient is much larger and more localized in the tachocline region than is seen in Figure 1. The exact shape of the curves, of course, depends on the tachocline model used and may not have much significance. The gradient in the latitudinal direction is significant only within the convection zone; this is of course expected, since this is where we find differential rotation. The maximum value of the latitudinal gradient is comparable to the radial gradient in the outer shear layer. This gradient is negative almost everywhere. When studying the temporal evolution of the two gradients, we compare the magnitude of the time variation with the corresponding time-averaged values.

Although the pattern of variation of these gradients is similar for results obtained with GONG and MDI data, the actual values show significant differences in some regions. The results obtained from the two data sets agree reasonably well as far as the latitudinal gradient is concerned, although there are differences at high latitudes. There are noticeable differences in the radial gradients obtained from the two data sets, particularly in the outer shear

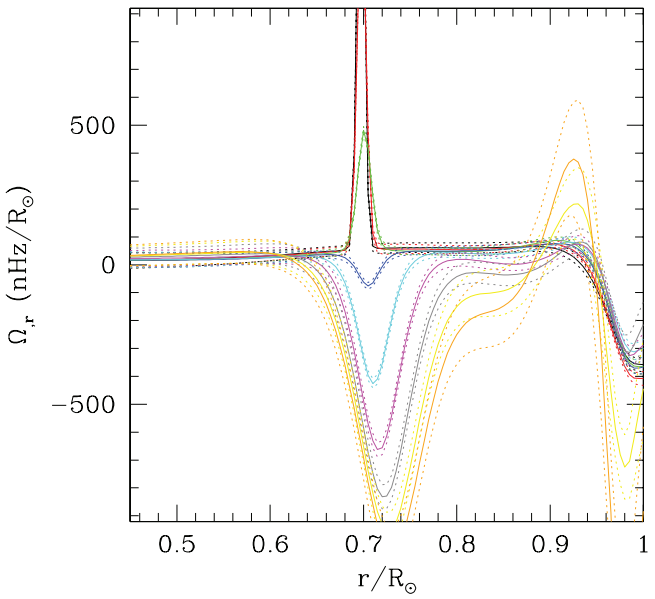

FIG. 2.—Mean radial gradient, Ω_r, obtained from MDI data using the tachocline model of Antia et al. (1998) shown at a few selected latitudes. The color scheme is the same as that in the upper row of Fig. 1. Error bars are shown by dotted lines.

layer. Such differences between results from GONG and MDI data have been seen even for the rotation rate itself (e.g., Schou et al. 2002), and the reasons for this disagreement are not fully understood. This issue is discussed further in connection with the temporal variations of the radial gradient.

3.1. *The Time Variation of the Rotational Velocity: The Zonal Flows*

Figure 3 shows the residual rotational velocity $\delta v_\phi = \delta\Omega r \cos\theta$ obtained using GONG data. Results are shown at a few representative radii in the convection zone. The figure shows the expected, distinct, bands of faster and slower than average rotation velocity that, at low latitudes, move toward the equator with time. At high latitudes, the bands seem to move toward the poles. The slow band at high latitudes reaches its end near the poles around 2001, the time when the polar field reversed, while the fast band at high latitude, on the other hand, appears to terminate around 1996 (and will probably do so again in 2008) near the minimum of solar activity. The transition between the equatorward and poleward movements takes place at a latitude of around 45°. At high latitudes it appears that the 12 years of GONG data have covered a little more than one period, but at low latitudes the periodicity of the zonal flow pattern is not obvious. The zonal flow pattern in the outer shear layer appears to be more complex at low latitudes than at high latitudes. In this layer, the low-latitude fast-moving bands from the two hemispheres appear to have merged around 2000, but seem to split around 2005, and then merge again in 2007. A band of fast rotation appears near a latitude of 35° in both hemispheres around 2005, and we believe that these bands are a precursor to the next solar cycle. In fact, a closer examination of the figure suggests that these bands have a weak connection to the bands that started at 50° latitude around 1997 and then bifurcated around 2004 into one branch that moved poleward and another that moved toward the equator. These bands should reach the equator and merge during the next maximum phase of solar activity. Thus, the band that started near the 50° latitude zone in 1997, i.e., just after the minimum phase of the activity, is expected to reach the equator during the maximum of the following cycle and will thus span a period of 15–18 yr. The band of slow rotation that started a few years after the last solar activity maximum around a latitude of 50° would reach the equator some time after the next minimum, again spanning a period of ~1.5 times the fiducial solar cycle.

Figure 3 also shows the zonal flow pattern obtained using GONG data as cuts at a few representative latitudes. These can be used to determine how the zonal flow pattern changes with radial distance. At low latitudes there is a clear trend of the pattern moving upward with time and it is also clear that the pattern

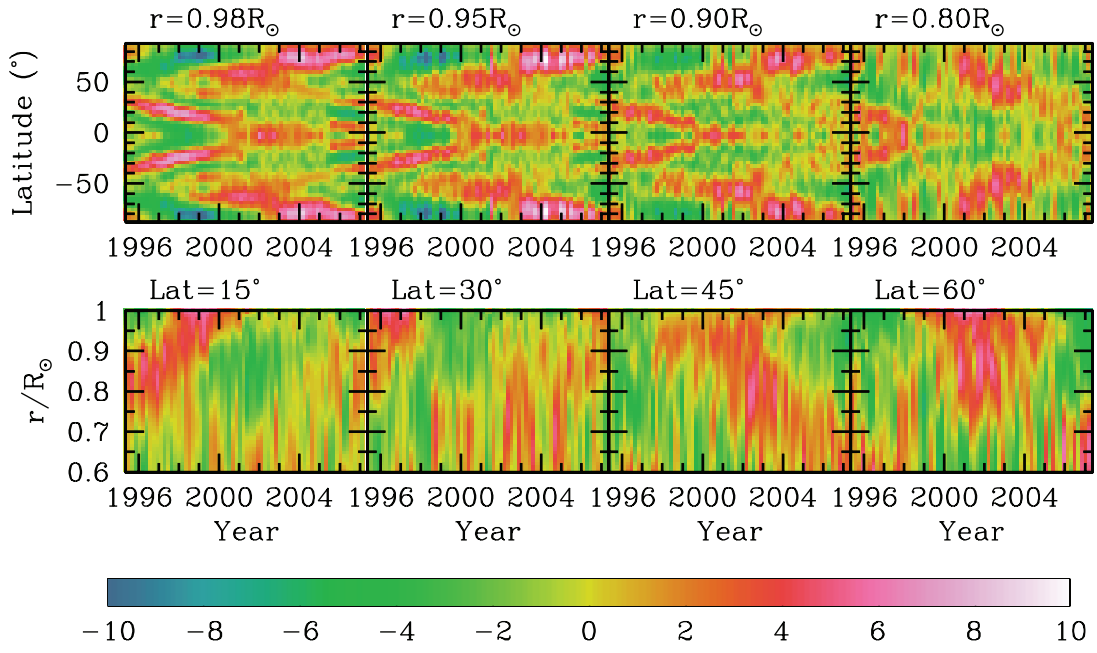

FIG. 3.—Diagrams showing δv_ϕ, the residuals of the rotation velocity obtained using GONG data. We show the results at a few representative depths and latitudes as marked above the respective panels. The scale is in m s^{-1}.

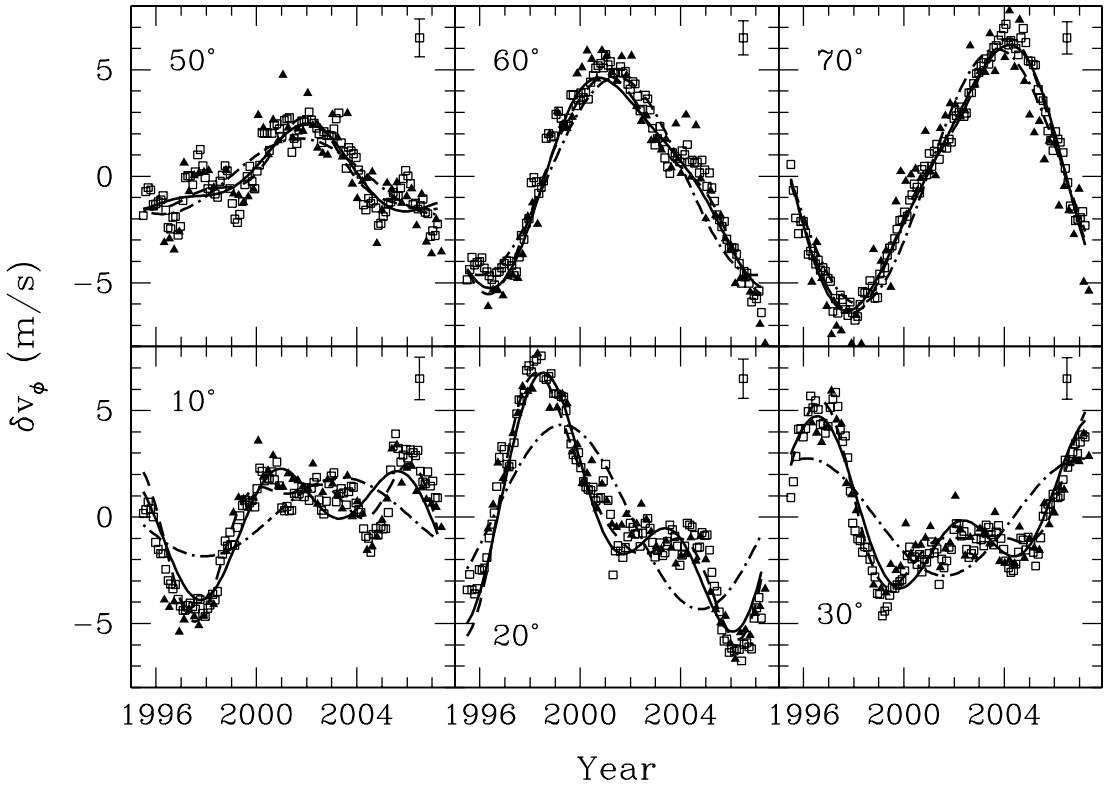

FIG. 4.—Zonal flow velocity as a function of time at different latitudes at $r = 0.98\ R_\odot$. The latitudes are marked in each panel. The squares show results obtained with GONG data, while triangles show results with MDI data. The dash-dotted, solid, and dashed lines show the fits using eq. (2) to the GONG results with 1, 2, and 3 terms, respectively. For clarity, error bars are not shown on the points; however, a typical error bar is shown by a point in the upper right corner of each panel.

penetrates through most of the convection zone, probably reaching down to the base of the convection zone. At these low latitudes the average rate of upward movement appears to be about $0.05\ R_\odot\ \mathrm{yr}^{-1}$, or about 1 m s^{-1}. This follows from the fact that Figure 3 shows the band moving from close to the base of the convection zone to surface in about 6 yr. Even at a latitude of 60°, the band of faster rotation appears to penetrate nearly to the base of the convection zone near the maximum of solar activity.

The changing pattern of the zonal flows implies that the maximum and minimum velocities of the flow occur at different times for different latitudes and depths. This has also been found by Schou (1999) and Howe et al. (2000a). Figure 4 shows the zonal flow velocity, δv_ϕ, at different latitudes as a function of time at $r = 0.98\ R_\odot$. Both GONG and MDI results are shown, and as can be seen, there is good agreement between the results obtained using data from the two projects. It is clear that the time dependence of δv_ϕ changes with latitude. While the high latitudes show a nearly sinusoidal variation with a possible period of close to 11 yr, the variation at low latitudes is more complicated. The Fourier transform of the results at all latitudes shows a peak at the lowest frequency bin, which corresponds to a period of about 11 yr. The pattern at low latitudes, however, is clearly not sinusoidal. Thus, if it is periodic, higher harmonics must be present. Vorontsov et al. (2002) and Basu & Antia (2003) had found the third harmonic to be important. But those studies were based on data covering only about half of the solar cycle. With more data, Howe et al. (2005) and Basu & Antia (2006) found the second harmonic to be more significant than the third harmonic. Clearly, data from cycle 24 will be needed to establish the periodicity properly. At a latitude of around 50°, the amplitude of the flows is distinctly smaller than that at other latitudes. This is close to the latitude where the switch from the equatorward movement to poleward movement of the flows occurs. Thus, regions around this latitude seem to separate the two branches of the zonal flow pattern.

While it is not possible to confirm the periodicity of the flows with current data sets, it is tempting to assume a period comparable to the average solar cycle. Thus, we assume that the pattern is periodic with a period of 11 yr and fit it using equation (2) with three terms. The amplitudes of the first two terms are shown in Figure 5 for results obtained from both GONG and MDI data. Both these data sets give similar results, and it is clear that although the amplitude of the dominant $k = 1$ component decreases with depth, the pattern appears to penetrate to the base of the convection zone. The highest amplitude, of up to 10 m s^{-1}, is seen in the outer $0.1\ R_\odot$ at high latitudes. The amplitude is small in the midlatitude region around 45°. It is clear that the $k = 2$ harmonic is significant; however, its magnitude is much smaller than that for the first term. The amplitude of the third term is found to be even smaller, and it is difficult to estimate the amplitude reliably. The relative magnitude of the various harmonics may depend on the origin of the zonal flow pattern. In the very deep layers close to the tachocline, the errors in the zonal flow velocity estimates are so large that it is difficult to assign any significance to the fluctuating results obtained there. Below the convection zone the amplitude of both harmonics is very small, indicating that solar-cycle-related variations are not clearly seen in these layers.

Figure 5 also shows the phase of the $k = 1$ term obtained from both GONG and MDI data. It is clear that at low latitudes the phase changes rather steeply around $r = 0.9\ R_\odot$. At high latitudes, while MDI results show very little phase variation with depth, GONG results do show some variations. It is not clear if these differences are significant. In the outer half of the convection

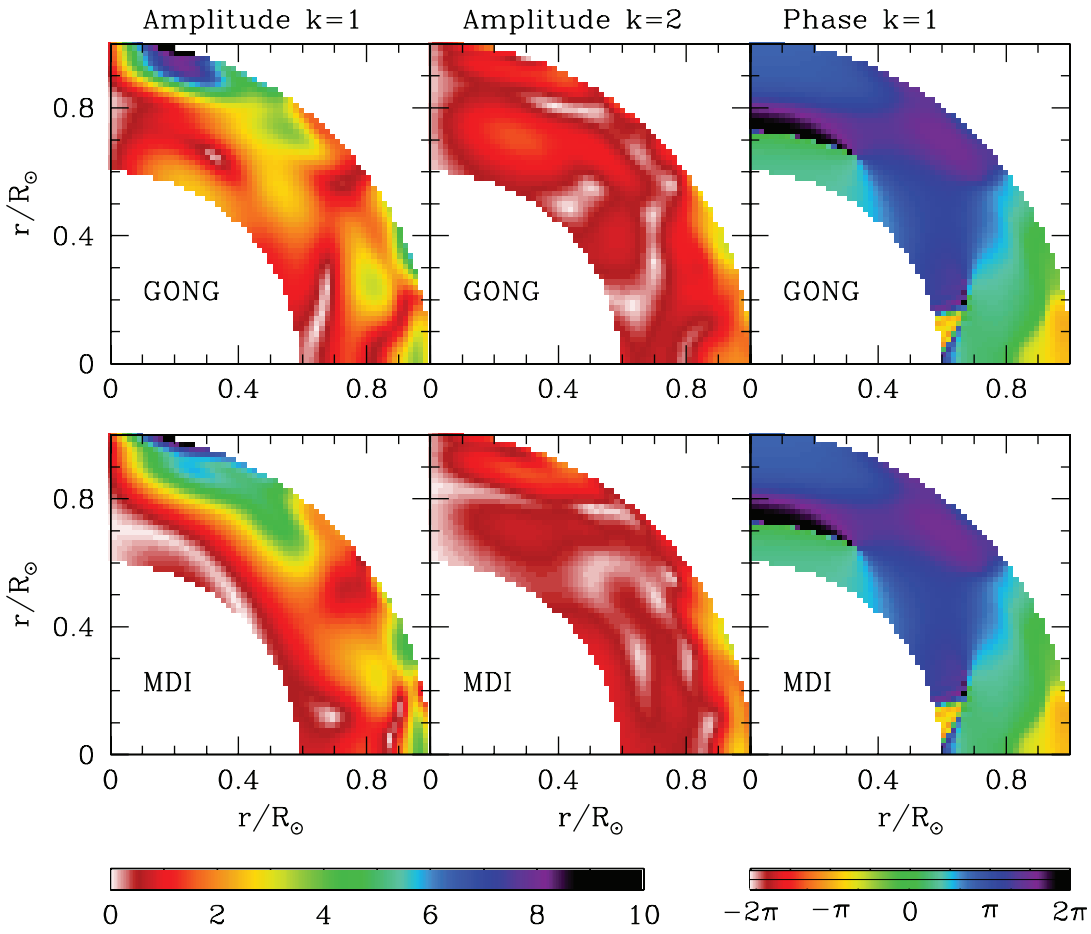

FIG. 5.—Diagram showing amplitudes of the $k = 1$ and 2 (eq. [2]) components and the phase of $k = 1$ component of zonal flow expansion as obtained using GONG and MDI data. For panels that show the amplitudes, the scale is in units of m s^{-1}.

zone, both GONG and MDI results appear to show a sharp transition around a latitude of 40°. This may mark the transition between the low- and high-latitude patterns. There is good agreement between the GONG and MDI results.

We can extend the zonal flow pattern over longer time intervals if we assume that the fitted parameters do not change from cycle to cycle, and the resulting pattern can be compared with predictions from different dynamo models. We shall be happy to make such figures available for investigators who wish to make use of them.

3.2. *Temporal Variations of the Rotation Rate Gradients*

We calculated the time variation of both radial and latitudinal gradients by numerical differentiation of the rotation rate residuals that were obtained using equation (1). Figures 6 and 7 show the two components of the gradient at different latitudes as a function of time at $r = 0.95\ R_\odot$. There is a reasonable agreement between results obtained using GONG and MDI data at this depth. It is clear that there is significant time variation in these gradients and that the amplitude of the variation is a sizable fraction of its average value. At low latitudes, the temporal variation of the radial gradient turns out to be about 20% of its average value. The relative variation in the latitudinal gradient is similar. These changes are much larger than the temporal variation in the rotation rate, which is only about 0.1%–1% of its average value. As a result, we expect this time variation in the angular velocity gradients to play an important role in workings of the solar dynamo.

In order to establish a possible relation between the zonal flow bands and the magnetic cycle, we compare the pattern of temporal variations of $\delta\Omega_r$ and $\delta\Omega_\theta$ at $r = 0.95\ R_\odot$ with the butterfly diagram seen in the distribution of sunspots. The results are shown in Figure 8. We have chosen this depth because GONG and MDI results for the radial gradient do not agree well in shallower layers. We have multiplied the gradients by $\cos\theta$ in this and subsequent figures in order to compensate for the increase in $\delta\Omega$ with latitude. This factor is already present in the residual rotation velocity δv_ϕ, since it is part of the conversion from Ω to v_ϕ. As a result of this factor residuals in v_ϕ show little variation in amplitude with latitude, and with this factor, residuals in $\delta\Omega_r$ or $\delta\Omega_\theta$ also show a similar behavior. It can be seen from Figure 8 that the sunspots are mainly concentrated in regions where the radial gradient is larger than its average value and where the latitudinal gradient is smaller than the average gradient. Note that the mean values of both these gradients are negative at this depth, and hence their magnitude will be larger in regions where $\delta\Omega_r$ or $\delta\Omega_\theta$ are negative. Thus, the sunspots are found to occur in regions where the magnitude of the radial gradient is smaller than average and that of the latitudinal gradient is larger than average. Clearly, the butterfly pattern is related to zonal flows, as was, indeed, noted earlier by Snodgrass (1987). Around 2005, when the equatorial zonal flow band of faster rotation splits, the latitudinal gradient of rotation rate flips sign in the low-latitude region.

The errors in our results on the gradients are naturally expected to be larger than those in $\delta\Omega$. These large errors give rise to some of the fluctuations seen in Figures 6 and 7. As in the case of δv_ϕ, these fluctuations can be smoothed by fitting a periodic signal with a period of 11 yr to the results using equation (2). The fitted

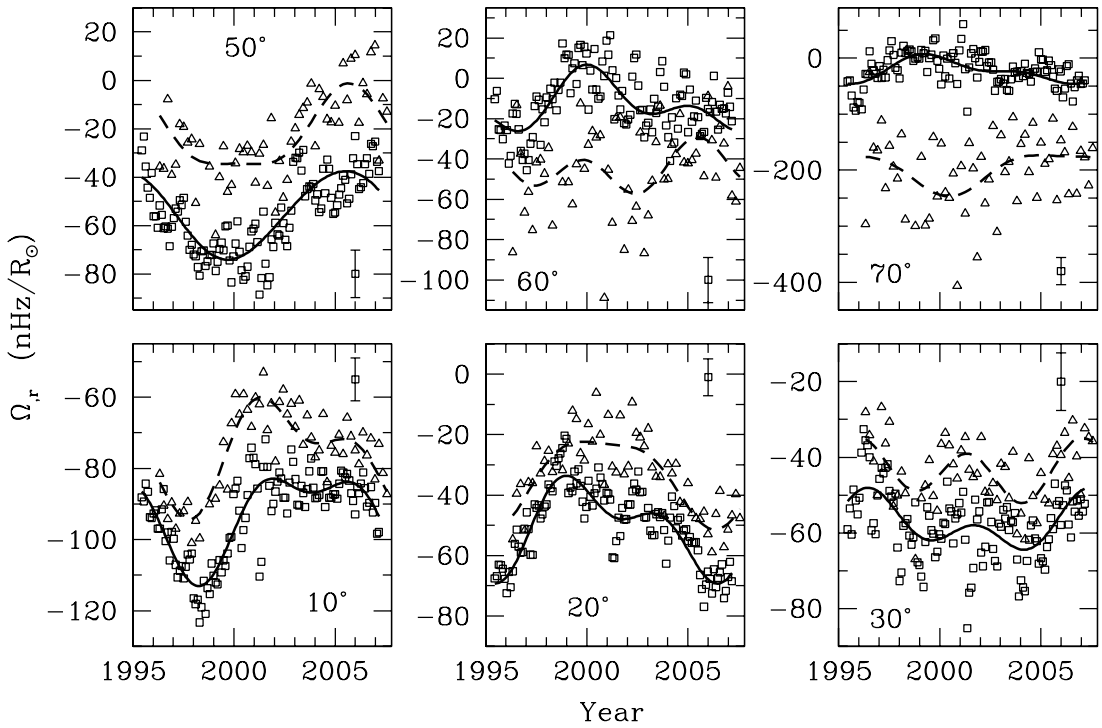

FIG. 6.—Radial gradient, Ω_r at a few selected latitudes for $r = 0.95\ R_\odot$. The squares and triangles show results obtained using GONG and MDI data, respectively. The solid and dashed lines show fits obtained using equations similar to eq. (2) to these points. For clarity, error bars are not shown on the points, but a typical error bar is shown by a point in a corner of each panel.

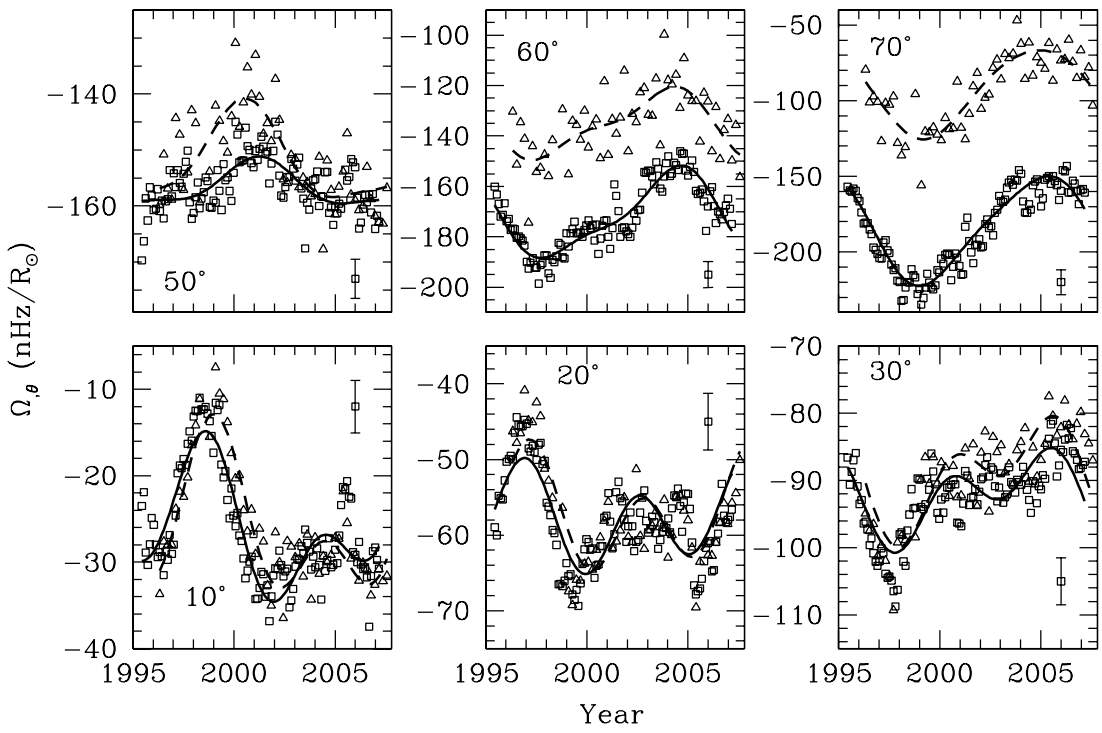

FIG. 7.—Same as Fig. 6, but for the latitudinal gradient Ω_θ.

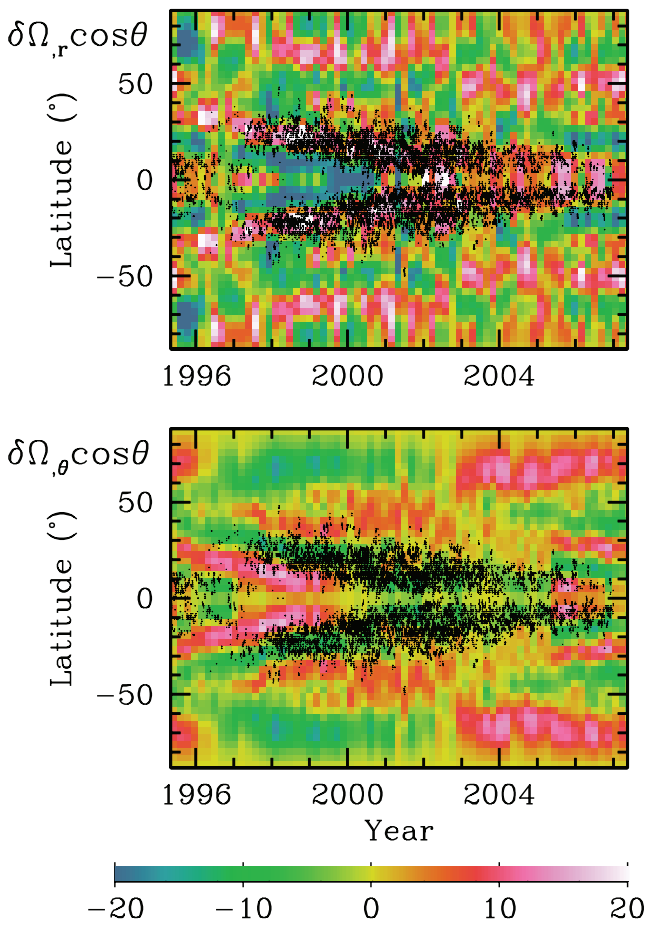

FIG. 8.—Radial and latitudinal gradients at $r = 0.95\ R_\odot$ superposed on the butterfly diagram showing the distribution of sunspots which is obtained from the Greenwich sunspot data. The scale is marked in nHz $R_\odot^{-1}$.

results, extended to a period of 22 yr, are shown in Figures 9 and 10. The pattern of bands of higher and lower than average gradients can be seen in these figures too, with low-latitude bands moving toward the equator, and the pattern once again changing at high latitudes. In general, there is reasonable agreement between GONG and MDI results, except in the case of the radial gradient at $r = 0.98\ R_\odot$, where there are significant differences between the two results.

The agreement between GONG and MDI results is better in deeper layers, despite the fact that the gradient itself is much smaller. As far as the latitudinal gradient is concerned, the agreement between GONG and MDI results is good at all depths. It has been known for some time that there are differences between GONG and MDI rotational splitting data (Schou et al. 2002). These differences result in the differences between results obtained with GONG and MDI data about the outermost layers at all latitudes. The most prominent difference is, however, in the radial gradient of the rotation rate at high latitudes. MDI data show the presence of a jetlike feature at high latitudes, while GONG data do not (e.g., Howe et al. 1998; Schou et al. 2002). Interestingly, the differences between the GONG and MDI data do not affect the time variations of the zonal flow velocities and the results obtained from the two different data sets agree reasonably well. This may indicate that the systematic differences between the two data sets are largely independent of time. Since we calculate the residual $\delta\Omega$ independently for GONG and MDI, the systematic errors cancel when the mean value is subtracted in equation (1).

It is tempting to speculate that the difference in radial gradient in the outer layers between the MDI and GONG results is because of the presence of higher degree modes, in particular the *f*-modes, in MDI data sets. To test this we repeated the calculations by removing these modes and find that the results remain largely unaffected. Thus, the difference between GONG and MDI results is unlikely to be due to the difference in resolution due to presence of extra modes and possibly represents the difference in splitting coefficients themselves as found by Schou et al. (2002). While the zonal velocity, δv_ϕ, computed using the two data sets agrees reasonably well, the time variation of the radial gradient of the inversions shows significant differences. Thus, the process of determining the radial gradient and its time variation appears to amplify the differences. In order to identify the modes that lead to this difference, we did one more set of inversions for MDI data using only modes with $\ell < 120$; the resulting radial gradient is closer to the result obtained using GONG data as can be seen from Figure 11. Thus, it is clear that the differences are caused by the high-degree modes in the MDI sets. Similar problems have been noticed in even-order splitting coefficients from MDI (Antia et al. 2003). A closer look at Figure 9 suggests that at $r = 0.98\ R_\odot$ there was a rather sharp change around 1999, which is around the period when contact with *SOHO* was re-established. This is similar to the results on asphericity found by Antia et al. (2003) and results on solar radius variations found by Antia (2003). All these could be due to some systematic error introduced during the recovery of *SOHO*. High-degree modes that are trapped in the outer layers do not seriously affect the inversion results in the deeper layers, and hence, these layers are not affected by the possible problems with the MDI high-degree modes. The reanalysis of MDI data has shown that there are some removable problems with the currently available data sets (Larson & Schou 2008).

The pattern at high latitudes is complicated, and it is not possible to say with any certainty whether the pattern is moving toward the poles or toward the equator. From Figure 9 it can be seen that at $r = 0.95\ R_\odot$, the band with lower than average radial gradient that started around a latitude of 50° in about 1995 ends at the equator around 2012, thus spanning a period of about one and a half fiducial solar cycles. This is similar to the corresponding band in the zonal flow pattern. However, unlike the bands in the zonal flow pattern, these bands appear to last for only about 1 solar cycle in the latitudinal gradient pattern. From the panels in Figure 9 that show the radial dependence of Ω_r it also appears that the pattern rises upward with time at low latitudes. At the latitude of 30° the amplitude of the variation in the radial gradient is rather small. This is the latitude where the radial gradient in the lower convection zone changes sign (cf. Fig. 1), and the magnitude of temporally averaged Ω_r is small too. At high latitudes (>45°) the bands showing the changes in the radial gradient penetrate to the base of the convection zone, while at low latitudes the amplitude decreases below the outer shear layer, and there is a distinct phase shift around $r = 0.9\ R_\odot$. For the latitudinal gradient, the temporal variations are generally significant only in the outer shear layer, and below a depth of $0.1\ R_\odot$ this component is generally small (Fig. 10).

3.3. *The Time Derivative of* v_ϕ

We evaluate the time derivative of δv_ϕ, the zonal flow velocity, by differentiating the fits in equation (2). The results are shown in Figure 12. As expected, the magnitude of the derivative is of the order of $\omega_0 |\delta v_\phi|$, i.e., about 10^{-7} m s^{-2}. Since this derivative is

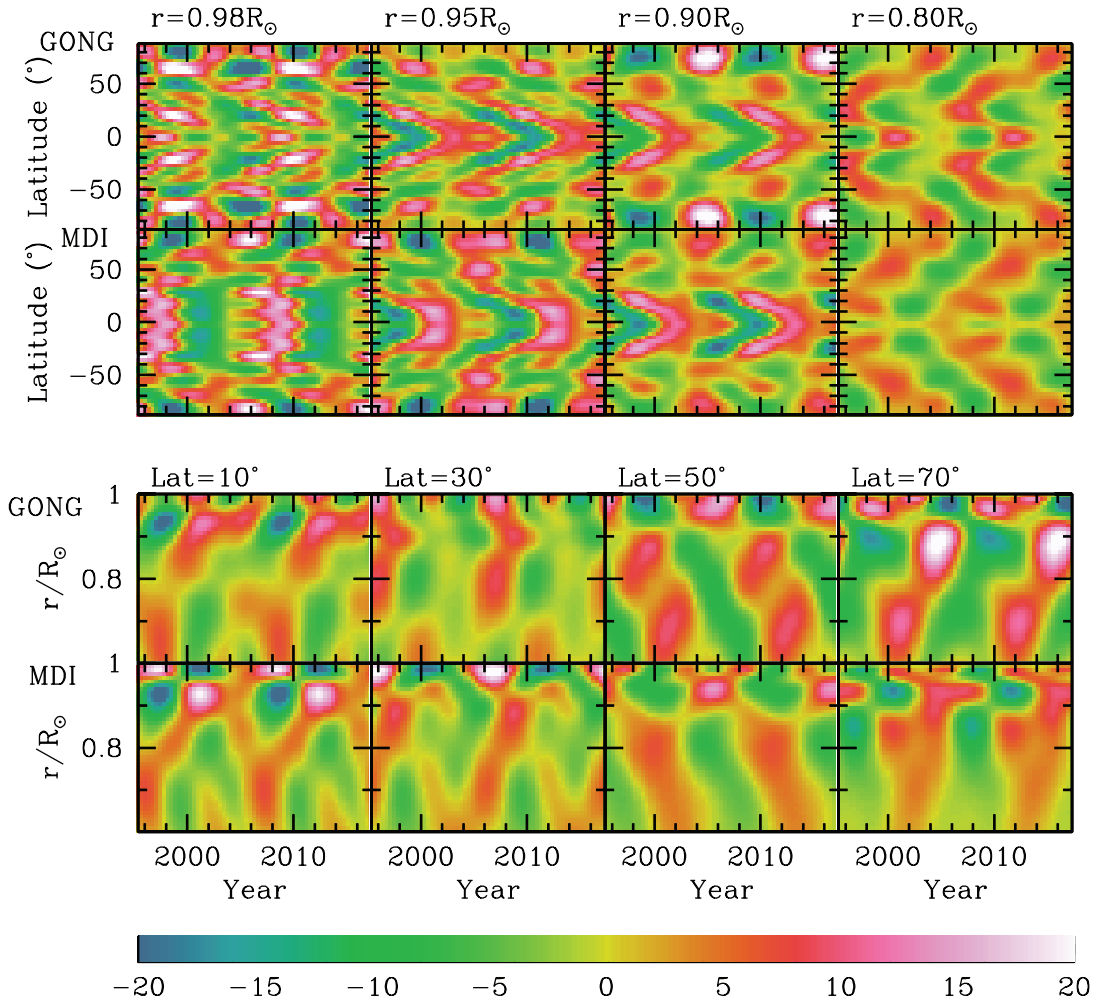

FIG. 9.—Residuals in the radial gradient obtained using GONG and MDI data at a few selected depths or latitudes. We actually show $\delta\Omega_r \cos\theta$ to minimize latitudinal variation. The scale is marked in units of nHz $R_\odot^{-1}$.

calculated by differentiating equation (2), the pattern of the derivative is essentially similar to that of δv_ϕ, except for a phase shift of $\pi/2$. However, the higher harmonics make a larger contribution to the zonal flow derivative than to the flow itself, and as a result, there are additional differences between the patterns that can be seen when the pattern of the zonal flow derivative is compared to the pattern of the zonal flow. The second and third harmonics appear to dominate in the deeper parts of the convection zone near the tachocline, but since the signal in this region is fairly weak even in δv_ϕ, it is not clear if this is significant.

4. DISCUSSION AND CONCLUSIONS

We have studied the time variation of the solar internal rotation rate and its gradients over almost the entire period covering solar cycle 23 using data from the GONG and MDI projects. We used the rotation rate residuals obtained by subtracting the time-averaged rotation rate from that at each epoch at a given latitude and depth to study the zonal flow pattern and to determine how it changes with time. These residuals have also been used to study the radial and latitudinal gradients of the zonal flows, as well as the time derivative of solar rotation velocity. Our main results are as follows:

1. The rotation velocity residuals show the well-known pattern similar to the observed pattern of torsional oscillations at the solar surface. At low latitudes the results show bands of faster and slower than average rotation speed moving toward the equator as the solar cycle progresses. At high latitudes on the other hand, these bands move toward the poles. The transition between the equatorward and poleward movement occurs around a latitude of 45°.

2. We find a precursor of the next solar cycle in the form of a band of fast rotation that appeared at about 35° latitude near the surface around 2005, when the Sun was approaching the activity minimum. We also find that the band of faster rotation found in the region near the equator appears to have bifurcated around the same time.

3. The zonal flow pattern at low latitudes moves upward, toward shallower depths, with an average speed of about 1 m s^{-1}.

4. The relative time variation of the radial gradient of the rotation rate is about 20% of its average value, which is much larger than the relative variation in the rotation rate itself. The time variation of the latitudinal gradient is large only in the outer 0.1 $R_\odot$ of the Sun, the maximum change being about 20% of the mean value.

5. The magnetic butterfly diagram coincides with a band of larger than average radial gradient and with smaller than average latitudinal gradient at $r = 0.95\ R_\odot$. Noting that both gradients are negative, the sunspot activity bands occur in regions of enhanced latitudinal shear and diminished radial shear, as compared to the magnitude of the average shear.

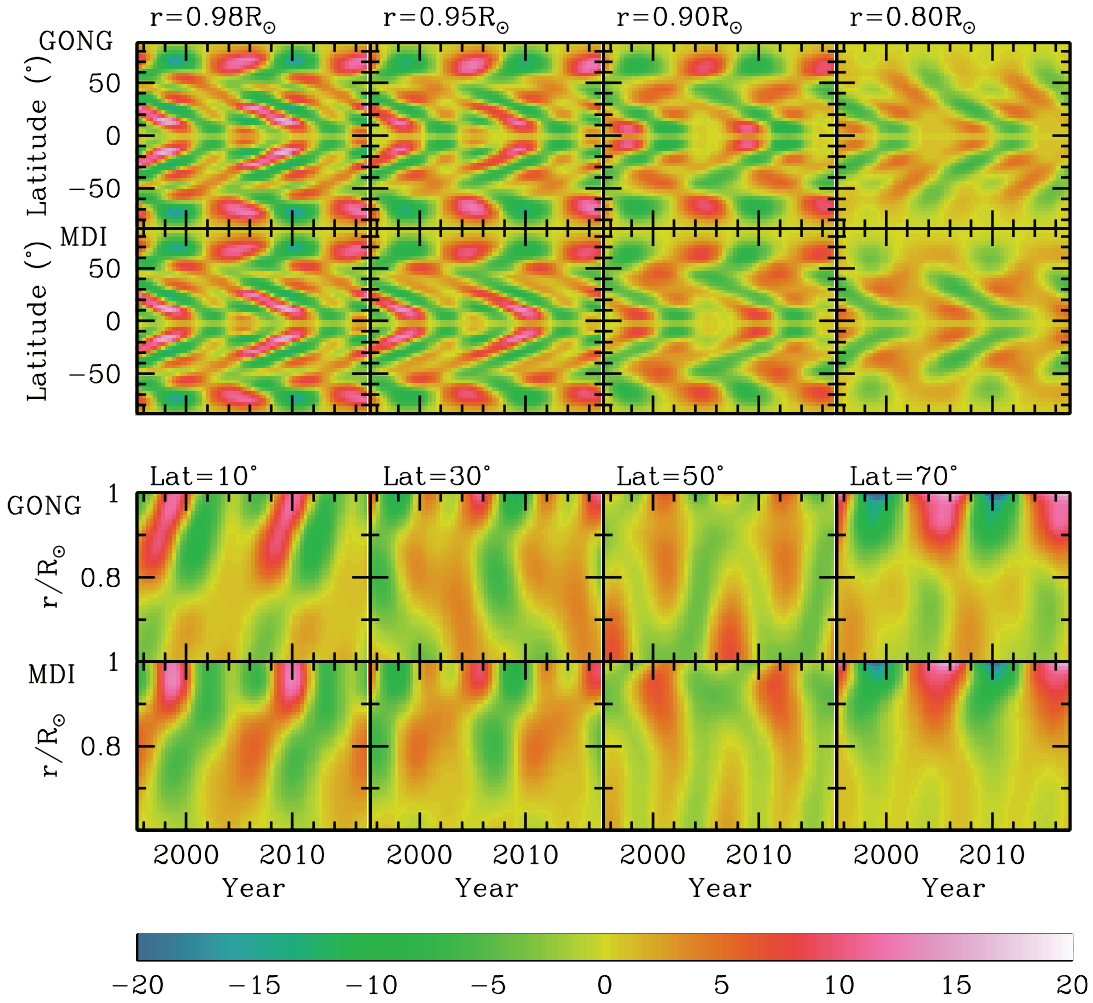

FIG. 10.—Residual in the latitudinal gradient obtained using GONG and MDI data at a few selected depths or latitudes. We actually plot $\delta\Omega_\theta \cos\theta$ to minimize latitudinal variation. The scale is marked in units of nHz $R_\odot^{-1}$.

6. The time derivative of the rotation velocity is about 10^{-7} m s^{-2}.

The equatorward movement of the zonal flow pattern at low latitudes is well known (Schou 1999; Howe et al. 2000a; Antia & Basu 2000; Vorontsov et al. 2002). The poleward migrating high-latitude branch has also been noted earlier by Antia & Basu (2001) and Ulrich (2001). The transition between the equatorward and poleward movements occurs around a latitude of 45°. The differences between the low- and high-latitude patterns also manifest in integrated quantities such as the rotational kinetic energy and angular momentum (Antia et al. 2008). The time variations of the rotational kinetic energy integrated separately over low- and high-latitude regions also differ. The high-latitude regions show a kinetic energy variation that is correlated with the solar activity throughout the convection zone. At the low latitudes, on the other hand, the positive correlation between kinetic energy and solar activity exists only in the outer 0.1 $R_\odot$, while the variations are anticorrelated with solar activity in the rest of the convection zone. Observations of magnetic features at the solar surface also show an equatorward movement at low latitudes (manifesting in the well-known butterfly diagram) and a poleward movement at high latitudes (e.g., Leroy & Noens 1983; Makarov & Sivaraman 1989; Erofeev & Erofeeva 2000; Benevolenskaya et al. 2001). Theoretical models of the solar dynamo, such as those of Covas et al. (2000, 2001) and Bushby (2005), show these features, although they do differ in detail, such as in the phase. The predicted butterfly diagrams of many models (Jiang et al. 2007; Rempel 2006) also show a low-latitude equatorward moving branch and a high-latitude poleward drifting branch.

The splitting of the band marking fast rotating region near the equator appears to be a new feature, and we are not aware of any other investigations that have noted this. Although we have shown only GONG results, MDI data also show the splitting of the bands. The observations during the last solar minimum, however, do not show this feature clearly. However, a closer look at Figure 3 shows a faint signature of two bands merging at the equator around 1996, albeit with a magnitude of δv_ϕ around 0.5 m s^{-1}, which is comparable to the error estimates and about a factor of 5 lower than the corresponding value around 2006. This difference could indeed be owing to cycle-to-cycle variation. We clearly need more data to see the development of this pattern. The near-surface behavior of zonal flows can be seen in the surface rotation rate data from Mt. Wilson (Ulrich 2001; Howe et al. 2006a) that also cover the previous solar cycle. Since the errors in these observations are larger, it is difficult to say whether the splitting of the near-equator band was seen in these results during the last cycle.

The rise of the zonal flow pattern with time has been seen in subsurface layers from other measurements too. Conclusions

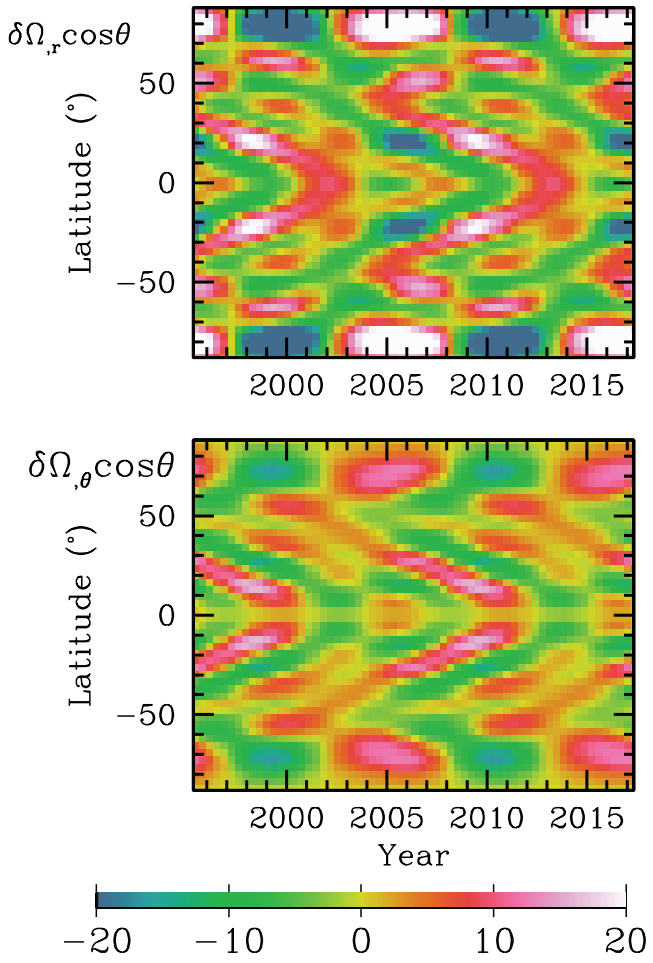

FIG. 11.—Residual in the radial and latitudinal gradient obtained at $r = 0.98\,R_\odot$ using MDI data with $\ell < 120$ modes. We actually plot $\delta\Omega_r \cos\theta$ and $\delta\Omega_\theta \cos\theta$ to minimize latitudinal variation. The scale is marked in units of nHz $R_\odot^{-1}$.

similar to ours were drawn by Komm et al. (1993), who compared the zonal flow pattern obtained using the Doppler measurements at the surface with that from magnetic features that are believed to be anchored underneath the surface. Our result that the zonal flows penetrate through a good fraction of the convection zone, and probably reach the base of the convection zone, appears to contradict early inferences (Howe et al. 2000a; Antia & Basu 2000) that these flows penetrate only to a radius of $0.9\,R_\odot$. The early results could have been due to the fact that the phase of the zonal flow pattern at low latitudes changes around this depth. With limited data this could have led to the conclusion that the pattern does not penetrate below this depth. This phase change is seen in the variation of rotational kinetic energy in low latitudes too (Antia et al. 2008). Our results are, however, similar to those of Vorontsov et al. (2002), Basu & Antia (2003), and Howe et al. (2005). Vorontsov et al. (2002) also found that a band of faster rotating elements appears to penetrate almost up to the base of the convection zone at latitude of around 60°. Dynamo models that assume that the tachocline is the seat of the dynamo (e.g., Covas et al. 2000, 2001, 2004; Bushby 2005) also predict that the zonal flow pattern should persist through the convection zone.

The possible link between time-dependent shear oscillation pattern and the solar activity cycle was first emphasized by Snodgrass (1987). This becomes evident from a striking resemblance of shear zones with the magnetic activity bands revealed through the butterfly diagram (Fig. 8). Making the assumption that the seat of the solar dynamo is likely to be located within the shear layers, the observational information that we have gained from the time variation of radial and latitudinal gradients of rotation rate should provide a valuable input for understanding the dynamo mechanism.

We have hitherto been concerned largely with the time variations of the global rotation rate, which are about 0.1%–1% of its mean value. The relative temporal variations in the radial and latitudinal gradients of the rotation rate, however, turn out to be larger, 20% or more of their mean values. Clearly, the time-varying shear pattern in the activity bands must play an important role in driving the magnetic cycle. In fact, the time derivatives of angular velocity may be used either as valuable input for dynamo models or at any rate as a constraint on them. Indeed, the time derivative of the differential rotation has been effectively used in dynamo models such as those of Covas et al. (2000) and Rempel (2006).

It is illustrative to consider the azimuthal components of the induction and momentum equations and neglect the presence of other velocity fields such as meridional circulation and dissipation, and write the equations

$$\frac{\partial B_\phi}{\partial t} = r\cos\theta \boldsymbol{B}_p \cdot \nabla\Omega, \tag{3}$$

$$\rho\,\frac{\partial v_\phi}{\partial t} = \frac{1}{4\pi r\cos\theta}\nabla\cdot\left[\boldsymbol{B}_p(r\cos\theta B_\phi)\right], \tag{4}$$

where $\boldsymbol{B}_p$ and B_ϕ are respectively the poloidal and toroidal components of the magnetic field, and ρ is the density, which is assumed to be independent of time (e.g., Basu & Antia 2000; Basu 2002). With the available knowledge of the time-dependent radial and latitudinal gradients of the angular velocity, it should be feasible to deduce the temporal variation of the toroidal magnetic field for an assumed configuration of the poloidal field. Equally, the force term can also be estimated using the measured acceleration $\partial v_\phi/\partial t$ provided we assume that the solar torsional oscillations are driven mainly by the Lorentz force, although there will be additional contributions from the temporally varying meridional flow (e.g., Haber et al. 2002; Basu & Antia 2003), which we neglect. To 1 order of magnitude we can write

$$\frac{\partial v_\phi}{\partial t} \approx \frac{|\boldsymbol{B}_p| B_\phi}{4\pi r\rho}. \tag{5}$$

If the magnitude of the poloidal field is estimated through independent means, it should be possible to infer the strength of the azimuthal field using our knowledge of $\partial v_\phi/\partial t$. Thus, if the magnitudes of both poloidal and toroidal components are comparable, then the magnetic field would be of the order of 1 G near the surface, increasing to 1000 G near the base of the convection zone. The surface value is consistent with observations of the average magnetic field at the surface (e.g., Ulrich & Boyden 2005). Since the magnetic field is generally concentrated in flux tubes with low filling factors, the magnetic field in these flux tubes is expected to be much higher. On the other hand, if the poloidal field is 100 times weaker than the toroidal field (e.g., Rempel 2007), then the toroidal field will be about 10 times the above estimate, i.e., of the order of 10 kG near the base of the convection zone.

In conclusion, we emphasize that observations of the zonal flows of the Sun now cover almost an entire solar cycle, and there are some features of the flows seen at this solar minimum phase that had not been noticed in the earlier solar minimum for

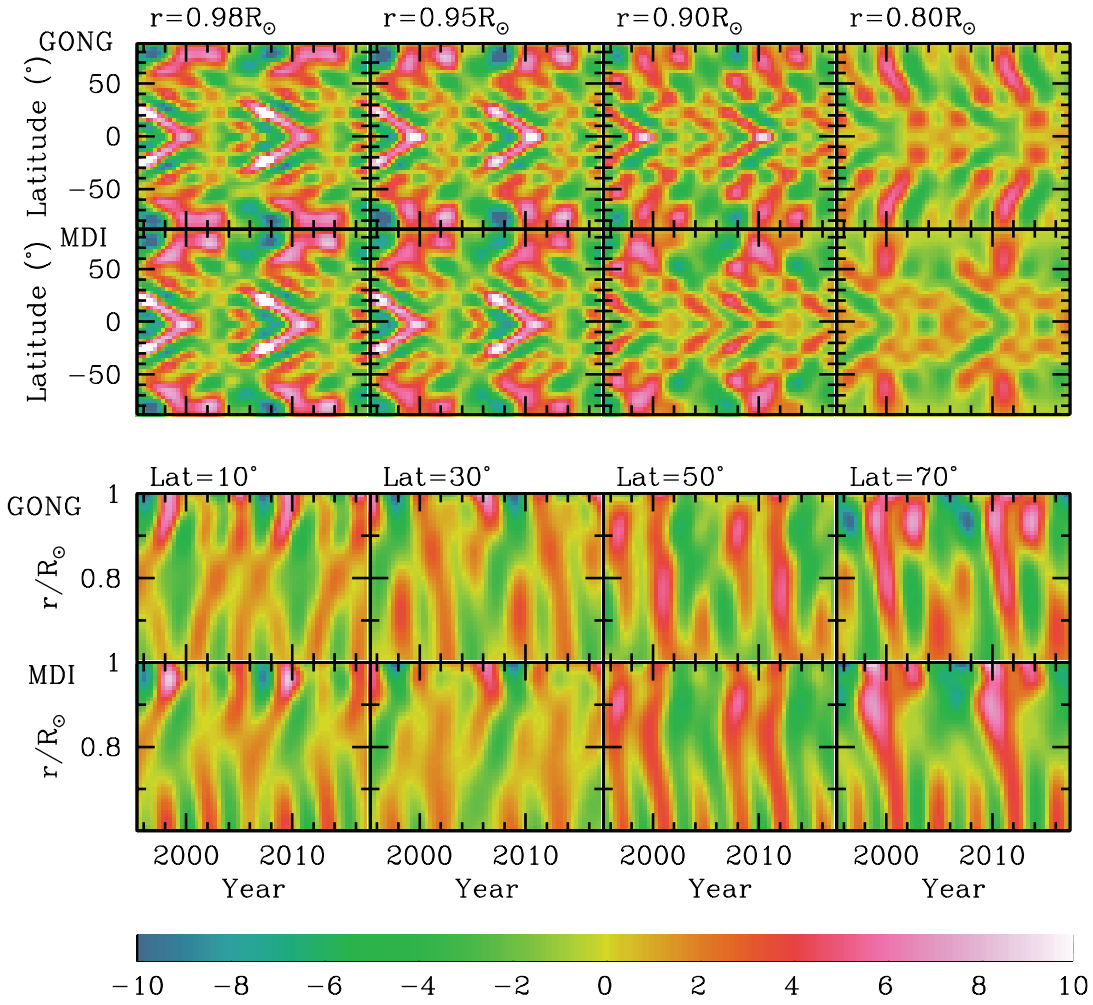

FIG. 12.—Acceleration $(1/\omega_0)\,\partial v_\phi\,\partial t$ obtained using GONG and MDI data at a few selected depths or latitudes. The scale is marked in units of m s^{-1}.

which the helioseismic data were sparse. The further evolution of these features should shed light on the differences between different solar cycles. The current results are also precise enough to provide important inputs to or constraints for solar dynamo models.

This work utilizes data obtained by the Global Oscillation Network Group (GONG) project, managed by the National Solar Observatory, which is operated by AURA, Inc., under a cooperative agreement with the National Science Foundation. The data were acquired by instruments operated by the Big Bear Solar Observatory, High Altitude Observatory, Learmonth Solar Observatory, Udaipur Solar Observatory, Instituto de Astrofisico de Canarias, and Cerro Tololo Inter-American Observatory. This work also utilizes data from the Solar Oscillations Investigation Michelson Doppler Imager (SOI/MDI) on the *Solar and Heliospheric Observatory* (*SOHO*). *SOHO* is a project of international cooperation between ESA and NASA. M. D. I. is supported by NASA grants NAG5-8878 and NAG5-10483 to Stanford University. S. B. acknowledges partial support from NSF grant ATM 0348837. S. M. C. thanks the Indian National Science Academy for support under the INSA Honorary Scientist programme.

REFERENCES

Antia, H. M. 2003, ApJ, 590, 567
Antia, H. M., & Basu, S. 2000, ApJ, 541, 442
———. 2001, ApJ, 559, L67
Antia, H. M., Basu, S., & Chitre, S. M. 1998, MNRAS, 298, 543
Antia, H. M., Chitre, S. M., & Gough, D. O. 2008, A&A, 477, 657
Antia, H. M., Chitre, S. M., & Thompson, M. J. 2003, A&A, 399, 329
Basu, S. 2002, in From Solar Minimum to Maximum, ed. A. Wilson (ESA SP-508; Noordwijk: ESA), 7
Basu, S., & Antia, H. M. 2000, Sol. Phys., 192, 449
———. 2001, in Proc. *SOHO* 10/GONG 2000 Workshop: Helio- and Asteroseismology at the Dawn of the Millennium, ed. A. Wilson (ESA SP-464; Noordwijk: ESA), 179
———. 2003, ApJ, 585, 553
———. 2006, in Proc. *SOHO* 18/GONG 2006/HELAS I, Beyond the Spherical Sun, ed. K. Fletcher & M. J. Thompson (SP-624; Noordwijk: ESA), 128
Benevolenskaya, E. E., Kosovichev, A. G., & Scherrer, P. H. 2001, ApJ, 554, L107
Bushby, P. J. 2005, Astron. Nachr., 326, 218
Corbard, T., & Thompson, M. J. 2002, Sol. Phys., 205, 211
Covas, E., Moss, D., & Tavakol, R. 2004, A&A, 416, 775
Covas, E., Tavakol, R., & Moss, D. 2001, A&A, 371, 718
Covas, E., Tavakol, R., Moss, D., & Tworkowski, A. 2000, A&A, 360, L21
Erofeev, D. V., & Erofeeva, A. V. 2000, Sol. Phys., 191, 281
Haber, D. A., Hindman, B. W., Toomre, J., Bogart, R. S., Larsen, R. M., & Hill, F. 2002, ApJ, 570, 855
Hill, F., et al. 1996, Science, 272, 1292
Howard, R., & LaBonte, B. J. 1980, ApJ, 239, L33
Howe, R., Antia, H., Basu, S., Christensen-Dalsgaard, J., Korzennik, S. G., Schou, J., & Thompson, M. J. 1998, in Proc. *SOHO* 6/GONG98, Structure and Dynamics of the Interior of the Sun and Sun-like Stars, ed. S. Korzennik & A. Wilson (SP-418; Noordwijk: ESA), 803

Howe, R., Christensen-Dalsgaard, J., Hill, F., Komm, R. W., Larsen, R. M., Schou, J., Thompson, M. J., & Toomre, J. 2000a, ApJ, 533, L163
———. 2000b, Science, 287, 2456
Howe, R., Christensen-Dalsgaard, J., Hill, F., Komm, R. W., Schou, J., & Thompson, M. J. 2005, ApJ, 634, 1405
Howe, R., Christensen-Dalsgaard, J., Hill, F., Komm, R. W., Schou, J., Thompson, M. J., & Toomre, J. 2007, Adv. Space Res., 40, 915
Howe, R., Komm, R. W., Hill, F., Ulrich, R., Haber, D. A., Hindman, B. W., Schou, J., & Thompson, M. J. 2006a, Sol. Phys., 235, 1
Howe, R., Rempel, M., Christensen-Dalsgaard, J., Hill, F., Komm, R. W., Larsen, R. M., Schou, J., & Thompson, M. J. 2006b, ApJ, 649, 1155
Jiang, J., Chatterjee, P., & Choudhury, A. R. 2007, MNRAS, 381, 1527
Komm, R. W., Howard, R. F., & Harvey, J. W. 1993, Sol. Phys., 143, 19
Kosovichev, A. G., & Schou, J. 1997, ApJ, 482, L207
Lanza, A. F. 2007, A&A, 471, 1011
Larson, T., & Schou, J. 2008, in Proc. Helioseismology, Asteroseismology, and MHD Connections (Bristol: IOP), in press
Leroy, J.-L., & Noens, J.-C. 1983, A&A, 120, L1
Makarov, V. I., & Sivaraman, K. R. 1989, Sol. Phys., 123, 367
Rempel, M. 2006, ApJ, 647, 662
———. 2007, ApJ, 655, 651
Ritzwoller, M. H., & Lavely, E. M. 1991, ApJ, 369, 557
Schou, J. 1999, ApJ, 523, L181
Schou, J., et al. 1998, ApJ, 505, 390
———. 2002, ApJ, 567, 1234
Snodgrass, H. B. 1987, Sol. Phys., 110, 35
———. 1992, in ASP Conf. Ser. 27, The Solar Cycle, ed. K. L. Harvey (San Francisco: ASP), 205
Spiegel, E. A., & Zahn, J.-P. 1992, A&A, 265, 106
Spruit, H. C. 2003, Sol. Phys., 213, 1
Thompson, M. J., et al. 1996, Science, 272, 1300
Ulrich, R. K. 2001, ApJ, 560, 466
Ulrich, R. K., & Boyden, J. E. 2005, ApJ, 620, L123
Ulrich, R. K., Boyden, J. E., Webster, L., Snodgrass, H. B., Padilla, S. P., Gilman, P., & Shieber, T. 1988, Sol. Phys., 117, 291
Vorontsov, S. V., Christensen-Dalsgaard, J., Schou, J., Strakhov, V. N., & Thompson, M. J. 2002, Science, 296, 101